ACS OMEGA

http://pubs.acs.org/journal/acsodf

Article

# Substrate-Induced Anisotropic Growth of $CuAlO_2$ Platelets in a Liquid−Solid Reaction

Cheng-Hung Shih, Cheng-Chia Chang, Kuang-Kuo Wang, Hui-Chun Huang, Liuwen Chang,* and Mitch M. C. Chou

Cite This: *ACS Omega* 2023, 8, 4703−4710

Read Online

ACCESS | Metrics & More | Article Recommendations

**ABSTRACT:** This study reports a simplified method to grow $CuAlO_2$ crystals of submillimeter sizes with a highly anisotropic shape of a platelet. The solid-state reaction of forming $CuAlO_2$ at ca. 1373 K in the first stage of the conventional flux method is no longer required. The $CuAlO_2$ platelets nucleated directly onto the $(0001)_{sapphire}$ surface in a melt of $Cu_2O$ saturated with $Al_2O_3$ at 1473 K. The excess flux was mostly removed by the capped alumina plate on cooling with a limited amount of residue which can be leached afterward. The $CuAlO_2$ platelets all have a 3R crystal structure with no line and planar defects observed by TEM. The $CuAlO_2$ crystals emit a luminescence at 3.49 eV associated with resonant Raman effect resulted from a band-to-band transition in room-temperature PL measurement. The facile fabrication method for growing highly anisotropic $CuAlO_2$ crystals paves the way for their practical application in photoelectrochemical devices.

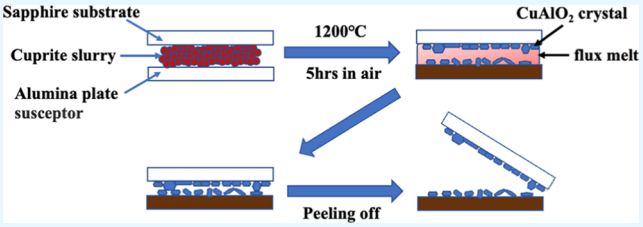


## INTRODUCTION

$CuAlO_2$ is a Cu-based delafossite-type compound which shows p-type conducting and optical transparent characteristics simultaneously.[1] This compound thus attracts great attention for applications in transparent electronic devices, such as transistors and diodes, by the formation of p−n junctions with n-type semiconductors which are abundantly available. In addition, the potential of $CuAlO_2$ to serve as an electrode in photoelectrochemical systems was also explored recently for solar water splitting,[2] chemical sensing,[3] and destructing pollutants in water.[4] It has been well recognized that the photocatalytic performance of an electrode material correlates strongly with its surface microstructure.[5] Sun et al.[6] suggested that flat $AgGaO_2$ particles capped mainly with electron-rich (0001) facets showed a 20-fold enhancement over the stretched $AgGaO_2$ ones in the reduction of benzyl bromide. $CuAlO_2$, as the same delafossite-type laminar compound as $AgGaO_2$, also possesses a high anisotropy of the electrical conductivity along the *a*- and *c*-axes.[7] It is thus preferable to fabricate $CuAlO_2$ crystals which are highly anisotropic in shape and to explore the anisotropy of the photocatalytic performance.

$CuAlO_2$ can be fabricated by techniques such as wet chemical synthesis including the hydrothermal[8] and sol−gel[9] methods and solid-state reaction of $Cu_2O/CuO$ and $Al_2O_3$.[10] The solid-state reaction method has been widely studied and used to fabricate $CuAlO_2$ powder without impurity phases. However, this method is both time and energy consuming and requires a well-controlled atmosphere.[11] In addition, the shape of the resultant crystals is not controllable. In order to obtain $CuAlO_2$ crystals in a larger size and with a well-faceted shape, a second treatment has to be performed by heating a mixture of $CuAlO_2$ and $Cu_2O/CuO$ to approximately 1473 K to obtain a solid−liquid melt and then cooling the melt slowly to 1323 K. This treatment is called the flux method, and well faceted crystals with millimeter sizes can be obtained.[11−13] The flux method relies on a straightforward solid−liquid reaction at temperatures ranging from ca. 1430 to ca. 1510 K to form an $Al_2O_3$-containing melt and $CuAlO_2$ seed crystals in which the seed $CuAlO_2$ crystals grew to larger sizes subsequently on cooling.[14,15] The resultant product is a mixture of $CuAlO_2$ and copper containing oxides such as $Cu_2O$, CuO, and $CuAl_2O_4$. A leaching process is therefore required afterward to remove the oxide flux.[11,12] Yoon et al.[13] proposed that the floating flux could be removed by creeping itself onto the wall of an alumina crucible during slow cooling; nevertheless, the shape of the $CuAlO_2$ crystals cannot be controlled. Recently, research conducted by Wolff et al.[15] pointed out that the crystallization of $CuAlO_2$ occurred in an $Al_2O_3$-containing melt of $Cu_2O$ upon cooling from 1473 K only in an atmosphere containing 25% $O_2$ or less. At higher $O_2$ contents, $CuAl_2O_4$ was the

Received: October 16, 2022
Accepted: January 20, 2023
Published: January 30, 2023

resultant phase. In addition, they found that the $Al_2O_3$ crucible was infiltrated by the melt, whereas the crucible made of sapphire stayed undamaged.

The present study is inspired by the above-mentioned results to develop a simplified flux method to grow anisotropic $CuAlO_2$ crystals in sub-millimeter sizes in a one-step heating treatment with a short soak time of a few hours. The platelets were formed with the assistance of the sapphire (0001) substrate having a highly anisotropic shape. These triangle or hexagonal platelets had sizes in the range of 50−150 $\mu$m and usually coalesced into aggregates of sub-millimeters or millimeters in size. The thinnest portion of the platelets, on the other hand, can be penetrated by high-energy electrons. The thickest portion of the platelet aggregates was estimated to be in the order of 10 $\mu$m.

## EXPERIMENTAL METHODS

Figure 1 shows a schematic drawing to demonstrate the processing sequences of the modified flux method for

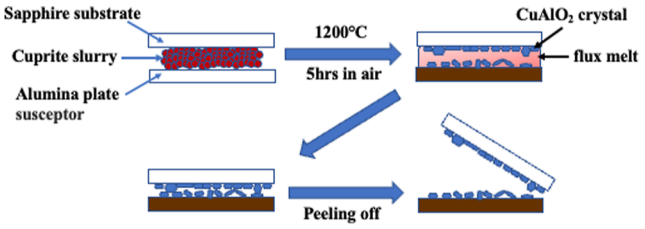


**Figure 1.** Schematic drawing of the modified flux method.

fabricating $CuAlO_2$ platelet crystals. First, cuprite powder (purity: 99%) was added into isopropanol under vigorous stirring to form a cuprite slurry. The slurry was pasted homogeneously onto a sintered alumina plate of 1 mm thickness by a syringe. The alumina plate overlaid with cuprite slurry was then covered by a sapphire (0001) substrate with the polished side facing the slurry to form a sandwich structure. The thickness of the cuprite slurry was estimated to be 0.1−0.5 mm. After that, the sandwich was loaded into a furnace, heated to 1473 K with a ramp rate of 0.5 K/s, socked for 5 h in air, and then cooled in the furnace. Last, the sapphire substrate and alumina plate were separated mechanically with $CuAlO_2$ crystals sticking loosely on both the alumina plate and the sapphire substrate. The crystals could be removed by a razor blade afterward. The residual cuprite flux was removed by dipping the sample in a 37% HCl solution for 30 min and rinsing with deionized water followed by blowing it to dry with nitrogen gas.

X-ray diffraction (XRD) was carried out using a Bruker D2 diffractometer equipped with Cu K$\alpha$ radiation to identify the phases in the calcined samples. The morphology of the resultant crystals was observed by optical microscopy and scanning electron microscopy (SEM, Zeiss Supra 55). Room-temperature photoluminescence (PL) measurements were conducted with a He−Cd 325 nm laser source to investigate the optical emission properties of the $CuAlO_2$ plates at room temperature. In addition, the optical phonon and strain of the plates were analyzed using a micro-Raman instrument equipped with a 532 nm laser source. The laser beam was focused through a microscope (50×, number aperture of 0.9) to a spot of 1 $\mu$m in diameter. The accumulation time was set to 360 s with two coadditions making the period of a scan run to about 24 min. The absorbance of grown samples was measured by an UV-Vis spectrometer using a xenon lamp light source. The compositions of the grown samples were determined by an energy-dispersive X-ray spectroscopy (EDS) instrument attached to the Supra 55 scanning electron microscope and a wavelength dispersive X-ray spectroscopy instrument attached to an electron probe micro-analyzer (EPMA, JEOL JXA-8530F). The microstructure of the $CuAlO_2$ microplate was also characterized by a field-emission transmission electron microscope (FE-TEM, FEI Tecnai G2 F20) operated at 200 kV. The cross-section TEM samples were prepared by the focus ion beam (FIB, Hitachi NX2000) technique.

## RESULTS AND DISCUSSION

Figure 2a shows the photograph of a peeled sapphire/alumina sandwich after calcination, revealing that the reaction products in black were spread over the alumina plate in a size which is larger than that of the sapphire substrate. The photograph of the peeled alumina/alumina sandwich is shown in Figure 2b for comparison. The surfaces of the sapphire substrate and alumina plate were examined by an optical microscope, and the

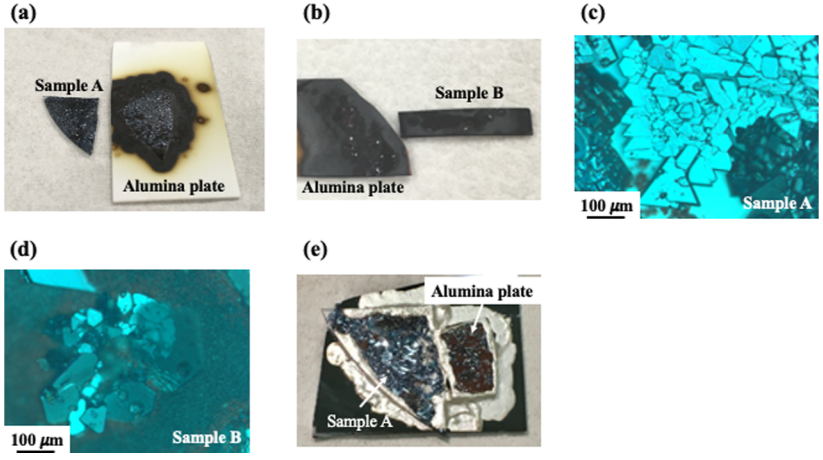


**Figure 2.** Photographs of an (a) as-peeled sapphire/alumina sandwich and (b) as-peeled alumina/alumina sandwich and optical micrographs of the (c) the sapphire [sample A labeled in (a)] and (d) alumina plate [sample B labeled in (b)] showing the $CuAlO_2$ crystals on them. Photographs of (e) sample A and alumina plate after 37% HCl solution leaching treatment.



https://doi.org/10.1021/acsomega.2c06672
ACS Omega 2023, 8, 4703−4710

results are shown in Figure 2c,d, respectively. It clearly reveals that the sapphire surface is overlaid with $CuAlO_2$ aggregates consisting of crystal platelets in triangular, rhombic, or hexagonal shapes with sizes in the range of 50−200 $\mu$m each. The size of an aggregate can be 1 mm or larger. On the other hand, the crystals on the alumina surface are mainly smaller than 50 $\mu$m and oriented randomly. The shape of the crystals coincides with the three- or six-fold symmetrical characteristics of $CuAlO_2$ having either a rhombohedral (3R) or hexagonal (2H) unit cells.[11] For the platelets in the same aggregate, their edges are all in parallel, indicating that the platelets not only possess a common ⟨0001⟩ direction (*c*-axis) parallel to the normal direction (ND) of the substrate but also are oriented consistently in the in-plane direction. A separate TEM observation for the platelets (results not shown) showed that the sapphire substrate (about 1 $\mu$m thick) itself reacted with the flux to form $CuAlO_2$. Accordingly, a preferential nucleation/growth of the $CuAlO_2$ platelets with a ⟨0001⟩// ND orientation can be induced by the presence of the (0001) sapphire substrate. The platelets are mainly capped by the {0001} surfaces. The {0001} surfaces of $CuAlO_2$, that is, the *ab*-plane, are the lowest resistivity crystal surface being 25 times larger than the *c*-axis resistivity at room temperature.[12] Figure 2e shows the photograph of the post leached samples. Compared to sample B, sample A shows a more profound blue coloration indicating that the flux has largely removed. A larger alumina substrate was used in purpose to absorb excess cuprite flux as much as possible to reduce the need for leaching, as shown in Figure 2e, and to prevent the overflow of the flux to contaminate the furnace.

The constituent phases of two samples, a sapphire substrate designated as sample A and an alumina plate designated as sample B, were examined by XRD, and the results are shown in Figure 3. It should be noted that $CuAlO_2$ has two

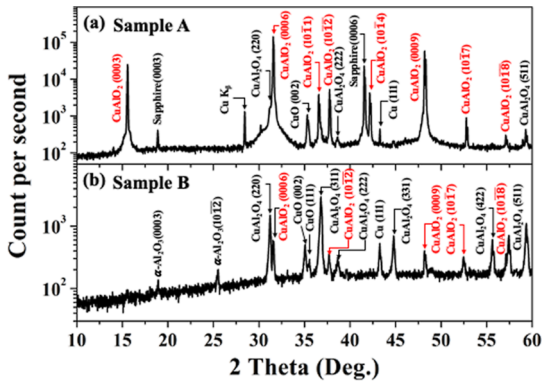


**Figure 3.** XRD patterns of (a) sample A and (b) sample B.

polymorphous phases with a rhombohedral (3R−$CuAlO_2$, $a = b = 2.8565$ Å, and $c = 16.9410$ Å)[16] and hexagonal (2H−$CuAlO_2$, $a = b = 2.863$ Å, and $c = 11.314$ Å)[16] crystal structure. The XRD pattern of sample A can be indexed predominantly as a 3R−$CuAlO_2$ phase with a strong preferred orientation of ⟨0001⟩//ND associated with the minor phases of Cu, CuO, and $CuAl_2O_4$. Since many peaks of the 3R and 2H phases overlap, it is difficult to exclude the presence of the 2H phase solely on the XRD result at the moment. The intensities of the strongest peaks of the minor phases are all 2 orders of magnitude less than that of the (0006) peak of $CuAlO_2$. Besides the {000*l*} peaks, the diffraction peaks of (10$\bar{1}$1), (10$\bar{1}$2), and (10$\bar{1}$4) of the $CuAlO_2$ phase located at 36.59, 37.76, and 42.28°, respectively, are also observed. The intensities of these peaks are much lower than that of the {0006} one, confirming that only a very small fraction of the $CuAlO_2$ crystals are oriented in such a way that their ⟨0001⟩ is not parallel to the ND. The diffraction pattern in Figure 3b shows that sample B contains the same phases. However, the diffraction peaks of the $CuAlO_2$ phase all have low intensities as compared to the sapphire counterpart, confirming that the $CuAlO_2$ crystals grew randomly on the alumina plate. In addition, the formation of the $CuAl_2O_4$ and CuO phases could be explained with two reasons. First, $Cu_2O$ reacted with $Al_2O_3$ during the temperature ramping in a low rate.[17] It was reported by Shy et al.[17] that the formation of $CuAl_2O_4$ could be avoided if the ramp rate was higher than 7 °C/s. In the present case, the ramp rate is 0.5 °C/s, far lower than the ramp rate needed. Second, $CuAlO_2$ decomposed into $CuAl_2O_4$ and CuO in a slow cooling.[18]

EPMA analysis was carried out for the $CuAlO_2$ platelets. Quantitative result showed that the atomic ratio of Cu and Al is 1.009, indicating that the oxide is slightly off-stoichiometric with slight deficiency in aluminum. Cu/Al ratios in the range of 0.96−1.08 have all been reported previously, revealing that no fixed trend of the ratio exists.[10,11,19] Figure 4a shows the secondary electron image of a platelet flake. The elemental maps in Figure 4b−d obtained from the EPMA analysis reveal that Cu, Al, and O distribute homogeneously in the crystal. A small area enriched with Al can be found in the upper-left corner of the platelet, indicating that a tiny piece of $CuAl_2O_4$ is attached to the crystal.

The distribution of $CuAlO_2$ platelets and second-phase particles on the sapphire substrate was further studied by SEM/EDS. Figure 5a shows the SEM micrograph of residue CuO distributed among the $CuAlO_2$ platelets and the corresponding EDS spectrum acquired from the highlighted position in the micrograph. In addition to the small amount of CuO residue, Figure 5b reveals that micrometer-sized $CuAl_2O_4$ crystals of an octahedron shape were occasionally found to be scattered on the $CuAlO_2$ platelets. Most of the second-phase particles can be removed by dipping the samples in a solution containing 37% HCl for 30 min. Figure 5c,d shows the SEM micrographs and EDS spectra of a leached sample, showing that a large portion of CuO and $CuAl_2O_4$ have been removed from the $CuAlO_2$ platelets. However, a very small amount of $CuAl_2O_4$ still remains in the gaps of the $CuAlO_2$ platelets. The residual quantity of $CuAl_2O_4$ can be estimated by XRD as shown in Figure 6a,b of the diffraction patterns of the sample prior to and after leaching, respectively. It clearly reveals that only three diffraction peaks of the $CuAl_2O_4$ phase, in addition to the peaks of sapphire and $CuAlO_2$, can be observed in very low intensities after leaching. The residues can be totally removed by prolonging the leaching time which is short as compared to that of the conventional method.[11]

Raman scattering analysis was conducted for $CuAlO_2$ grown on the sapphire substrate to identify the true crystal structure of the $CuAlO_2$ crystals obtained in the present study. Table 1 lists all possible Raman peaks for five Cu oxides and $\alpha$-$Al_2O_3$ for reference. Figure 7 shows the Raman spectrum acquired from the as-grown sample using a 532 nm laser in the region of 100−1000 $cm^{-1}$. Only one peak at 763 $cm^{-1}$ is observed and is assigned to be the $A_{1g}$ peak of the 3R phase resulted from the vibration of the O−Cu−O bond along the *c*-axis.[20−23] The appearance of only one vibrational mode in a backscatter


https://doi.org/10.1021/acsomega.2c06672
ACS Omega 2023, 8, 4703−4710

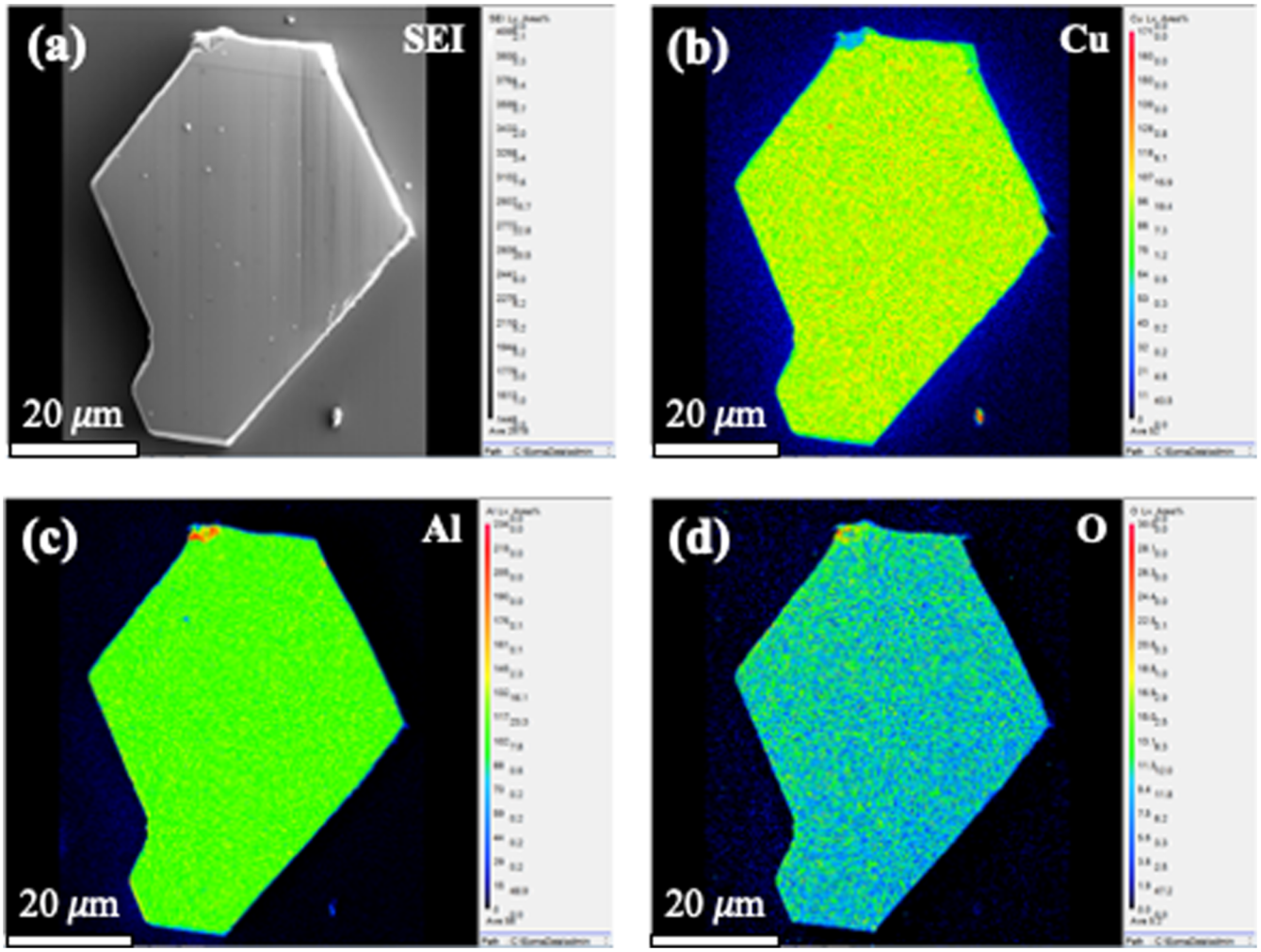


**Figure 4.** EPMA analysis for a $CuAlO_2$ micro-platelet flake placed on a Si substrate: (a) secondary electron image, (b) copper map, (c) aluminum map, and (d) oxygen map.

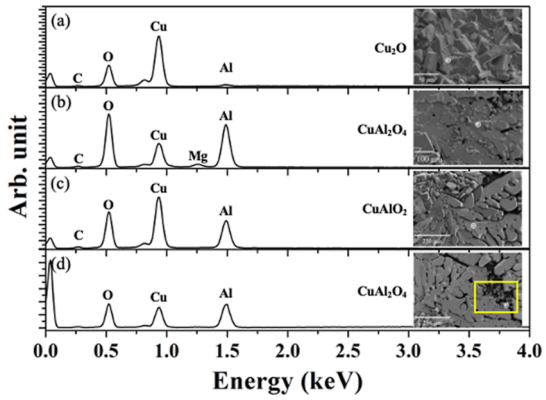


**Figure 5.** SEM micrographs and corresponding point EDS spectra of (a) CuO residue, (b) scattered $CuAl_2O_4$ on $CuAlO_2$, (c) $CuAlO_2$ after leaching, and (d) residual $CuAl_2O_4$ in the gap after leaching.

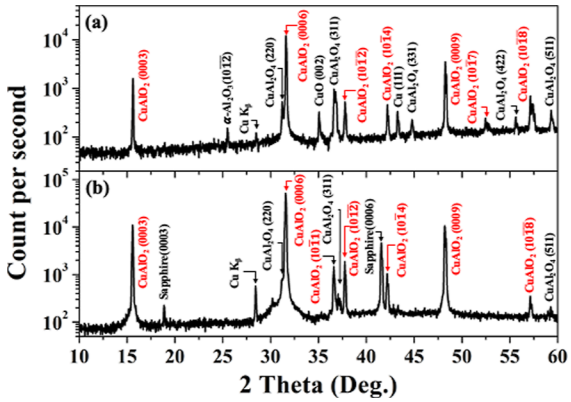


**Figure 6.** XRD patterns of a sapphire substrate (a) prior to and (b) after leached in a 37% HCl solution for 30 min.

geometry is due to the single-crystal nature of the sample. In other words, the size of the crystal is larger than the irradiated beam of 10 $\mu$m in diameter. No second phases as precipitates are present in the $CuAlO_2$ platelet. An enlarged drawing for the $A_{1g}$ peak is shown in the inset of Figure 7, revealing that a weak shoulder located at 767 $cm^{-1}$ is present. The shoulder can be attributed from either a slight distortion of the O−Cu−O bond in a portion of the crystal because of the oxygen deficiency[23] or the presence of planar defects or 2H precipitates.[23,24]

TEM analysis was also conducted to identify the crystal structure and microstructure of the $CuAlO_2$ platelets. The platelets peeled off from the sapphire substrate were first loaded on a Cu grid as shown by an optical micrograph in Figure 8a. The tip of a crystal (see the yellow circle in Figure 8a) can be penetrated by an electron beam, and its bright-field



https://doi.org/10.1021/acsomega.2c06672
ACS Omega 2023, 8, 4703−4710

**Table 1. Wavenumbers of Raman Peaks of Cu Oxides and Cu−Al Oxides Reported in the Literature**[20−23]

| phase | Raman shift (cm−1) | references |
|---|---|---|
| CuO | 297, 345, 632 | 20 |
| $\alpha$-$Al_2O3$ | 378, 418, 432, 451, 578, 648, 755 | 20 |
| $CuAl_2O_4$ | 476, 505, 610, 712, 792 | 20 |
| $Cu_2O$ | 154, 221, 434, 515, 635 | 21 |
| 3R−$CuAlO_2$ | 419, 610, 656, 763 | 2022, |
| 2H−$CuAlO_2$ | 119, 227, 262, 418, 498, 617, 659, 712, 767 | 23 |

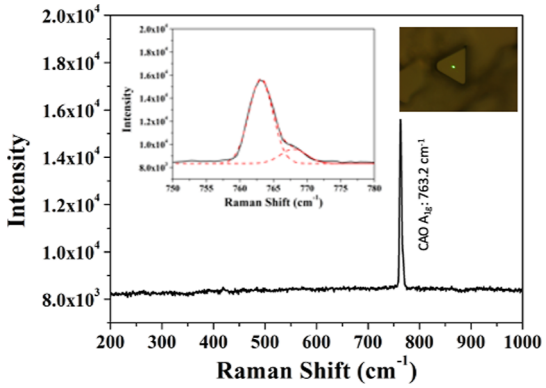


**Figure 7.** Raman spectrum of a $CuAlO_2$ platelet with an enlarged spectrum near 765 $cm^{-1}$ and a photograph showing the crystal in the inlet.

image is shown in Figure 8b. The corresponding diffraction pattern in Figure 8c reveals a [0001] zone axis with six $\{11\bar{2}0\}$ spots and corresponding Kikuchi bands. No $\{10\bar{1}0\}$ spots, which are present in the [0001] pattern of the 2H phase, are found. Moreover, Figure 8d demonstrates the bright-field image of a cross-section sample made by the FIB technique. In both the bright-field images in Figure 8b,d, no contrast resulted from planar or line defects is observed. The dislocation density of the crystal should therefore be less than $1 \times 10^8$ $cm^2$. The corresponding selected area electron diffraction patterns in Figure 8e can be indexed as a $[21\bar{3}0]$ zone with a c/a ratio of 3.95, coinciding with that of the 3R phase. Figure 8f shows a high-resolution micrograph with the (0003) fringes. All evidence shown above supports the conclusion that the $CuAlO_2$ platelets have a 3R crystal structure with a low density of crystalline defects and no presence of the 2H phase. In order to check whether the low density of dislocations observed by TEM is a local exception, Williamson−Hall analysis was conducted using the XRD data in Figure 3a. The strain obtained from the slope of the $\beta \cos\theta$ versus $\sin\theta$ plot was $9 \times 10^{-5}$. The dislocation density was also estimated as $2-3 \times 10^8$ $cm^{-2}$ which is very close to that obtained from TEM analysis.[25]

The optical band gap of the $CuAlO_2$ crystals was estimated by the absorption spectrum and PL spectrum acquired at room temperature. Figure 9 shows the absorption spectrum of a HCl-treated sample. The optical band gap, $E_g$, was determined by the Tauc plot method

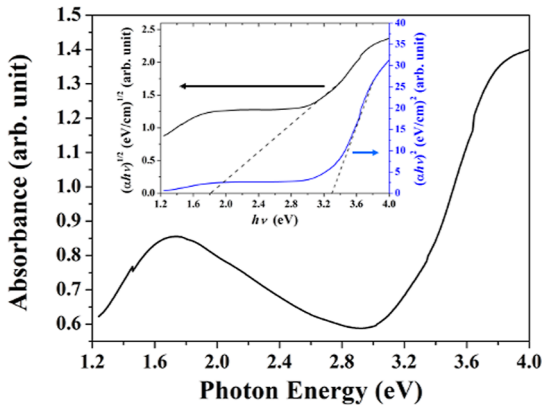


**Figure 9.** Absorbance spectrum of a HCl-treated $CuAlO_2$ sample. The inset shows the Tauc plots of $(\alpha h\nu)^2$ vs $h\nu$ and $(\alpha h\nu)^{1/2}$ vs $h\nu$ for estimation of the direct and indirect band gaps, respectively.

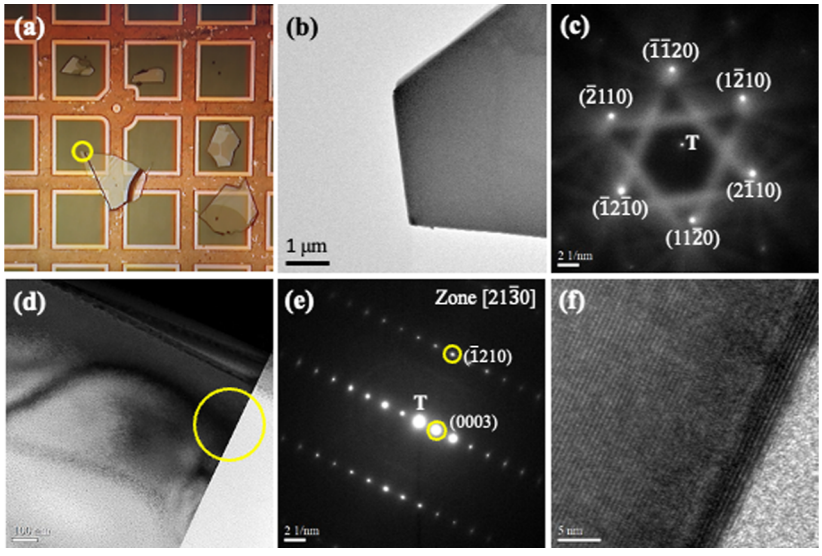


**Figure 8.** (a) Optical micrograph of $CuAlO_2$ platelets on a Cu grid, (b) plane-view TEM bright-field image of $CuAlO_2$ at the yellow circle in (a), and (c) corresponding diffraction pattern of the platelet tip. (d) TEM bright-field image of a $CuAlO_2$ cross-section sample, (e) corresponding selected-area diffraction pattern showing a $[21\bar{3}0]$ zone axis, and (f) corresponding high-resolution TEM image of the platelet. "*T*" in (c,e) indicates the transmitted electron beam.



https://doi.org/10.1021/acsomega.2c06672
ACS Omega 2023, 8, 4703−4710

$$(\alpha h\nu)^n = A(h\nu - E_g)$$

where $h\nu$ is the incident photon energy, $A$ is a constant, and the exponent $n$ is the type of optical transition, $n = 1/2$ for indirect and $n = 2$ for direct transition.[17] The direct and indirect optical band gap energies of $CuAlO_2$ platelets were determined from the intercept on $h\nu$-axis to be 3.3 and 1.8 eV, as shown in the inset in Figure 9. The direct optical band gap of 3.3 eV is lower than that of 3.5 eV reported.[1] The low band gap value cannot be a result interfered by the presence of $CuAl_2O_4$ which has an optical band gap of 2.1 eV.[26]

Figure 10 shows the PL spectra of single-crystal $CuAlO_2$ acquired from *c*- and *a*-planes, respectively. The *a*-plane sample

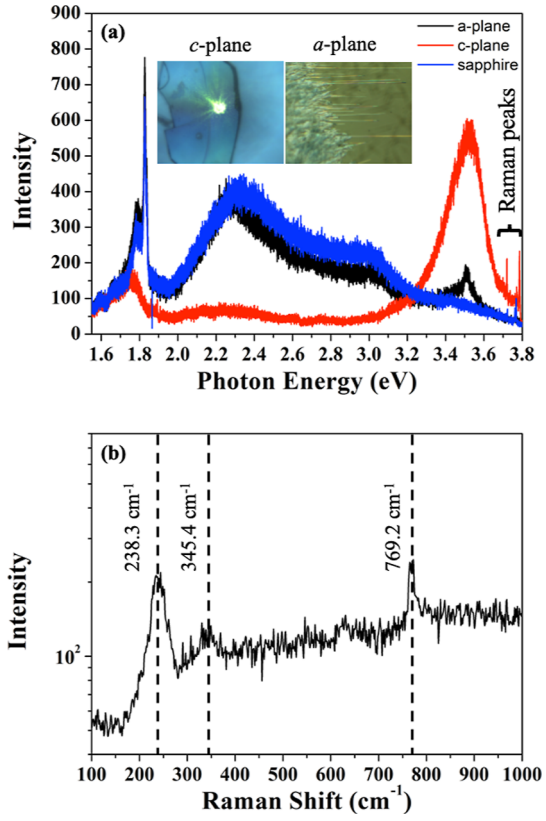


**Figure 10.** (a) Room-temperature PL spectrum and (b) Raman shift/wavelength conversion spectrum of $CuAlO_2$ microplate crystal.

was obtained in a trial run with different processing parameters. Two luminescence emission peaks are observed at 3.49 eV (355 nm) which are attributed to a near band gap emission (NBE) of $CuAlO_2$.[27] Another peak at 1.76 eV (704.5 nm) is attributed to the internal transitions of $Cu^{2+}$ ion in a field of low symmetry[27] but not secondary order band (710 nm). Comparing the direct band gap difference between PL and absorbance, the larger optical band gap of 3.49 eV is due to a transition within the direct band gap at the *L*-point, but the smaller optical band gap of 3.30 eV might be due to an indirect band gap transition within *L* to the Γ-point.[27,28] It is worth noting that the NBE of the *a*-plane is more than five folds lower than that of that of the *c*-plane, indicating a large anisotropy of PL existing between the *c*-axis and *ab* axes. The presence of the anisotropy in electron conduction and photoemission should provide advantages for devices made on the *c*-plane platelets.[29] The big hump distributed between 2 and 3 eV and a sharp peak at 1.82 eV resulted from the sapphire substrate. In addition, we also found the non-zero wavevector phonon Raman lines via resonance effects in Figure 10a. To inspect the detail of the near resonant Raman lines, we performed Raman shift/wavelength conversion, and the near resonant Raman spectrum is present in Figure 10b. Three pronounced peaks at 238.3, 345.4, and 769.2 $cm^{-1}$ are found. The 769.2 $cm^{-1}$ peak is consistent with the theoretical value of 770 $cm^{-1}$.[30] The 345.4 $cm^{-1}$ peak is associated with CuO ($A_g + 2B_g$),[20] whereas the origin of 238.3 $cm^{-1}$ peak is not clear yet. Byrne et al.[20] have also found a similar 236.5 $cm^{-1}$ peak in the study of the luminescent properties of $CuAlO_2$ powders. They speculated that the 236.5 $cm^{-1}$ peak may be associated with intrinsic crystalline vibrational modes as opposed to defect modes at sub-band gap excitation. Further studies are needed to clarify the origin of 238.3 $cm^{-1}$ peak.

According to the results reported by Wolff et al.,[15] the $Cu_2O$ slurry started to melt at a temperature slightly higher than 1273 K, and the content of $Al_2O_3$ in the melt increased gradually by dissolving the surface of the alumina plate. A small amount of $CuAlO_2$ might have crystallized upon soaking since a peritectic melting of $CuAlO_2$ has been observed in a $Al_2O_3$-containing melt of $Cu_2O$ at ca. 1500 K upon heating. The nucleation of platelet-like $CuAlO_2$ crystals is evidently induced by the (0001) sapphire surface. According to the classic nucleation theory, the activation of heterogeneous nucleation ($\Delta G_{het}$) of $CuAlO_2$ on $(0001)_{sapphire}$ can be expressed as

$$\Delta G_{het} = \frac{16\pi\gamma_{SL}^3}{3\Delta G_v^2} S(\theta)$$

where $\gamma_{SL}$ is the interfacial energy of $CuAlO_2$ nucleus and the melt, $\Delta G_v$ is the volume free energy, and $S(\theta)$ is a function of the contact angle of $\theta$. Among the parameters, only the contact angle is a function of the three interfaces. Among them, the interface between the $CuAlO_2$ nucleus and the alumina/sapphire substrate probably plays a major role. The $(0001)_{sapphire}$ surface has the lowest surface energy among the four low index surfaces of (0001), $(11\bar{2}0)$, $(10\bar{1}0)$, and $(1\bar{1}02)$.[31] The interfacial energy of the $(0001)_{CuAlO2}/(0001)_{sapphire}$ interface may be also to the lowest among all possible combinations. In addition, no epitaxy between $CuAlO_2$ and sapphire is observed. The formation of the $CuAlO_2$ platelets is therefore a result of preferential nucleation. By properly controlling the cooling rate, the size of the platelets can be further enlarged. On the other hand, it is evident that the $CuAlO_2$ crystals that nucleated on the alumina plate were randomly oriented and have a finer size, indicating that the nucleation is postponed due to the lack of sites having a low activation energy.

## CONCLUSIONS

This study demonstrated a simplified method to grow $CuAlO_2$ crystals of submillimeter sizes with an anisotropic shape of the platelet. The solid-state reaction of forming $CuAlO_2$ at ca. 1373 K in the first stage is no longer required. The $CuAlO_2$ platelets nucleated directly onto the $(0001)_{sapphire}$ surface in a melt of $Cu_2O$ saturated with $Al_2O_3$ at 1200 °C. The excess flux was mostly removed by the capped alumina plate on cooling with a limited amount of residue which can be leached afterward. The $CuAlO_2$ platelets all have a 3R crystal structure with no line and planar defects observed by TEM. The $CuAlO_2$ crystals emit a luminescence at 3.49 eV associated with resonant Raman effect resulted from a band-to-band transition


https://doi.org/10.1021/acsomega.2c06672
ACS Omega 2023, 8, 4703−4710

in room-temperature PL measurement. The facile fabrication method for growing highly anisotropic $CuAlO_2$ crystals paves the way for their practical application in photoelectrochemical devices.

## AUTHOR INFORMATION


### Corresponding Author

**Liuwen Chang** − *Department of Materials and Optoelectronic Science, National Sun Yat-sen University, Kaohsiung 80424 Taiwan, ROC; Center for Crystal Researches, National Sun Yat-sen University, Kaohsiung 80424 Taiwan, ROC;* orcid.org/0000-0002-1874-1566; Email: lwchang@mail.nsysu.edu.tw

### Authors

**Cheng-Hung Shih** − *Department of Materials and Optoelectronic Science, National Sun Yat-sen University, Kaohsiung 80424 Taiwan, ROC; Center for Crystal Researches, National Sun Yat-sen University, Kaohsiung 80424 Taiwan, ROC*

**Cheng-Chia Chang** − *Department of Materials and Optoelectronic Science, National Sun Yat-sen University, Kaohsiung 80424 Taiwan, ROC*

**Kuang-Kuo Wang** − *Department of Materials and Optoelectronic Science, National Sun Yat-sen University, Kaohsiung 80424 Taiwan, ROC*

**Hui-Chun Huang** − *Department of Materials and Optoelectronic Science, National Sun Yat-sen University, Kaohsiung 80424 Taiwan, ROC*

**Mitch M. C. Chou** − *Department of Materials and Optoelectronic Science, National Sun Yat-sen University, Kaohsiung 80424 Taiwan, ROC; Center for Crystal Researches, National Sun Yat-sen University, Kaohsiung 80424 Taiwan, ROC*

Complete contact information is available at: https://pubs.acs.org/10.1021/acsomega.2c06672


### Author Contributions

L.C.: Conceptualization, formal analysis, methodology, supervision, project administration, and writing. C.-H.S.: Investigation, formal analysis, and validation. C.-C.C.: Investigation and formal analysis. K.-K.W.: Investigation. H.C.H.: Investigation. M.M.C.C.: Project administration

### Notes

The authors declare no competing financial interest.

## ACKNOWLEDGMENTS

This work was supported by the Ministry of Science and Technology of the Republic of China (MOST-107-2221-E-110 -004 -MY3) and the M-era.net project (MOST 108-2923-M-110-006-MY3).

## REFERENCES


(1) Kawazoe, H.; Yasukawa, M.; Hyodo, H.; Kurita, M.; Yanagi, H.; Hosono, H. P-type electrical conduction in transparent thin films of $CuAlO_2$. *Nature* **1997**, *389*, 939−942.

(2) Choi, S. Y.; Kim, C. D.; Han, D. S.; Park, H. Facilitating hole transfer on electrochemically synthesized p-type $CuAlO_2$ films for efficient solar hydrogen production from water. *J. Mater. Chem. A* **2017**, *5*, 10165−10172.

(3) Tong, B.; Meng, G.; Deng, Z.; Horprathum, M.; Klamchuen, A.; Fang, X. Surface oxygen vacancy defect engineering of p-$CuAlO_2$ via Ar&$H_2$ plasma treatment for enhancing VOCs sensing performances. *Chem. Commun.* **2019**, *55*, 11691−11694.

(4) Lyu, L.; Yan, D.; Yu, G.; Cao, W.; Hu, C. Efficient Destruction of Pollutants in Water by a Dual-Reaction Center Fenton-like Process over Carbon Nitride Compounds Complexed Cu(II)-$CuAlO_2$. *Environ. Sci. Technol.* **2018**, *52*, 4294−4304.

(5) Dai, C.; Tian, X.; Nie, Y.; Lin, H. M.; Yang, C.; Han, B.; Wang, Y. Surface Facet of $CuFeO_2$ Nanocatalyst: A Key Parameter for $H_2O_2$ Activation in Fenton-Like Reaction and Organic Pollutant Degradation. *Environ. Sci. Technol.* **2018**, *52*, 6518−6525.

(6) Sun, Y.; Li, Y.; Li, Z.; Zhang, D.; Qiao, W.; Li, Y.; Niemantsverdriet, H.; Yin, W.; Su, R. Flat and Stretched Delafossite $\alpha$-$AgGaO_2$: Manipulating Redox Chemistry under Visible Light. *ACS Catal.* **2021**, *11*, 15083−15088.

(7) Lee, M. S.; Kim, T. Y.; Kim, D. Anisotropic electrical conductivity of delafossite-type $CuAlO_2$ laminar crystal. *Appl. Phys. Lett.* **2001**, *79*, 2028−2030.

(8) Thirumalairajan, S.; Mastelaro, V. R. A novel organic pollutants gas sensing material p-type $CuAlO_2$ microsphere constituted of nanoparticles for environmental remediation. *Sens. Actuators, B* **2016**, *223*, 138−148.

(9) Ohashi, M.; Iida, Y.; Morikawa, H. Preparation of $CuAlO_2$ Films by Wet Chemical Synthesis. *J. Am. Ceram. Soc.* **2002**, *85*, 270−272.

(10) Ingram, B. J.; González, G. B.; Mason, T. O.; Shahriari, D. Y.; Barnabè, A.; Ko, D.; Poeppelmeier, K. R. Transport and Defect Mechanisms in Cuprous Delafossites. 1. Comparison of Hydrothermal and Standard Solid-State Synthesis in $CuAlO_2$. *Chem. Mater.* **2004**, *16*, 5616−5622.

(11) Ishiguro, T.; Kitazawa, A.; Mizutani, N.; Kato, M. Single-crystal growth and crystal structure refinement of $CuAlO_2$. *J. Solid State Chem.* **1981**, *40*, 170−174.

(12) Tate, J.; Ju, H. L.; Moon, J. C.; Zakutayev, A.; Richard, A. P.; Russell, J.; McIntyre, D. H. Origin of p-type conduction in single-crystal $CuAlO_2$. *Phys. Rev. B: Condens. Matter Mater. Phys.* **2009**, *80*, 165206.

(13) Yoon, J. S.; Nam, Y. S.; Baek, K. S.; Park, C. W.; Ju, H. L.; Chang, S. K. Growth and properties of transparent conducting $CuAlO_2$ single crystals by a flux self-removal method. *J. Cryst. Growth* **2013**, *366*, 31−34.

(14) Jacob, K. T.; Alcock, C. B. Thermodynamics of $CuAlO_2$ and $CuAl_2O_4$ and Phase Equilibria in the System Copper(I) Oxide-Copper(II) Oxide-Aluminum Oxide. *J. Am. Ceram. Soc.* **1975**, *58*, 192−195.

(15) Wolff, N.; Klimm, D.; Siche, D. Thermodynamic investigations on the growth of $CuAlO_2$ delafossite crystals. *J. Solid State Chem.* **2018**, *258*, 495−500.

(16) Miclau, M.; Miclau, N.; Banica, R.; Ursu, D. Effect of polymorphism on photovoltaic performance of $CuAlO_2$ delafossite nanomaterials for p-type dye-sensitized solar cells application. *Mater. Today: Proc.* **2017**, *4*, 6975−6981.

(17) Shy, J. H.; Tseng, B. H. A novel method for preparing $CuAlO_2$ thin films and the film properties. *J. Phys. Chem. Solids* **2008**, *69*, 547−550.

(18) Neumann-Spallart, M.; Pinto, R. Growth conditions of $CuAlO_2$ films — Thermodynamic considerations. *Thin Solid Films* **2011**, *520*, 1299−1302.

(19) Mudenda, S.; Kale, G. M.; Hara, Y. R. S. Rapid synthesis and electrical transition in p- type delafossite $CuAlO_2$. *J. Mater. Chem. C* **2014**, *2*, 9233−9239.

(20) Byrne, D.; Bennett, N.; Cowley, A. The role of annealing conditions on the low temperature photoluminescence properties of $CuAlO_2$. *J. Lumin.* **2016**, *170*, 212−218.

(21) Ning, W.; Xia, C.; Xiaolan, C.; Yanjun, X.; Lin, G. Porous cuprite films: Facile solution deposition and their application for nitrite sensing. *Analyst* **2010**, *135*, 2106−2110.

(22) Suriwong, T.; Thongtem, T.; Thongtem, S. Thermoelectric and optical properties of $CuAlO_2$ synthesized by direct microwave heating. *Curr. Appl. Phys.* **2014**, *14*, 1257−1262.

(23) Baratto, C.; Kumar, R.; Faglia, G.; Vojisavljević, K.; Malič, B. p-Type copper aluminum oxide thin films for gas-sensing applications. *Sens. Actuators, B* **2015**, *209*, 287−296.
(24) Tanta, R.; Lindberg, C.; Lehmann, S.; Bolinsson, J.; Carro-Temboury, M. R.; Dick, K. A.; Vosch, T.; Jespersen, T. S.; Nygård, J. Micro-Raman spectroscopy for the detection of stacking fault density in InAs and GaAs nanowires. *Phys. Rev. B* **2017**, *96*, 165433.
(25) Metzger, T.; Höpler, R.; Born, E.; Ambacher, O.; Stutzmann, M.; Stömmer, R.; Schuster, M.; Göbel, H.; Christiansen, S.; Albrecht, M.; Strunk, H. P. Defect structure of epitaxial GaN films determined by transmission electron microscopy and triple-axis X-ray diffractometry. *Philos. Mag.* **1998**, *77*, 1013−1025.
(26) Salavati-Niasari, M.; Davar, F.; Farhadi, M. Synthesis and characterization of spinel-type $CuAl_2O_4$ nanocrystalline by modified sol−gel method. *J. Sol-Gel Sci. Technol.* **2009**, *51*, 48−52.
(27) Nam, Y. S.; Yoon, J. S.; Ju, H. L.; Chang, S. K.; Baek, K. S. Temperature-dependent Photoluminescence of $CuAlO_2$ Single Crystals Fabricated by Using a Flux Self-removal Method. *J. Korean Phys. Soc.* **2014**, *65*, 1068−1072.
(28) Pellicer-Porres, J.; Segura, A.; Gilliland, A. S.; Muñoz, A.; Rodríguez-Hernández, P.; Kim, D.; Lee, M. S.; Kim, T. Y. On the band gap of $CuAlO_2$ delafossite. *Appl. Phys. Lett.* **2006**, *88*, 181904.
(29) Chen, H.-Y.; Yang, Yu-C.; Lin, H.-W.; Chang, S.-C.; Gwo, S. Polarized photoluminescence from single GaN nanorods: Effects of optical confinement. *Opt. Express* **2008**, *16*, 13465−13475.
(30) Pellicer-Porres, J.; Martínez-García, D.; Segura, A.; Rodríguez-Hernández, P.; Muñoz, A.; Chervin, J. C.; Garro, N.; Kim, D. Pressure and temperature dependence of the lattice dynamics of $CuAlO_2$ investigated by Raman scattering experiments and ab initio calculations. *Phys. Rev. B: Condens. Matter Mater. Phys.* **2006**, *74*, 184301.
(31) Stirner, T.; Sun, J.; Aust, M. Ab initio Hartree-Fock simulation of r-plane sapphire. *Phys. Procedia* **2012**, *32*, 635−639.


https://doi.org/10.1021/acsomega.2c06672
*ACS Omega* 2023, 8, 4703−4710